Dynamics of fluorine ions in LaF_3-type crystals investigated by NMR lineshape analysis

2006 J. Phys.: Condens. Matter 18 1725

(http://iopscience.iop.org/0953-8984/18/5/025)

INSTITUTE OF PHYSICS PUBLISHING JOURNAL OF PHYSICS: CONDENSED MATTER

J. Phys.: Condens. Matter **18** (2006) 1725–1741 doi:10.1088/0953-8984/18/5/025

Dynamics of fluorine ions in LaF_3-type crystals investigated by NMR lineshape analysis

D Kruk[1,2,3], O Lips[2], P Gumann[2], A Privalov[2] and F Fujara[2]

[1] Institute of Physics, Jagiellonian University, Reymonta 4, 30-059 Krakow, Poland
[2] Institut für Festkörperphysik, TU Darmstadt, Hochschulstraße 6, 64289 Darmstadt, Germany

E-mail: Danuta.Kruk@physik.tu-darmstadt.de

Received 29 July 2005
Published 20 January 2006
Online at stacks.iop.org/JPhysCM/18/1725

Abstract

Fluorine nuclear magnetic resonance (NMR) lineshape data were collected for a pure LaF_3 single crystal and $La_{1-x}Sr_xF_{3-x}$ single crystals, doped with admixtures concentrations x up to 16%, from room temperature up to 775 K. The experimental data are analysed within the framework of a theoretical model linking the shape of the spectrum to parameters describing motional processes in the system. The elaborated model includes various types of the fluorine dynamics: diffusion processes occurring inside two distinct fluorine sublattices and inter-lattice exchange motion. This theoretical approach provides a satisfactory and consistent interpretation of the NMR data, without assuming any distribution of the characteristic time constants. The obtained results are discussed in a context of Arrhenius temperature dependences of the correlation times and effects caused by higher concentrations of the admixtures.

1. Introduction

The high mobility of fluorine ions in LaF_3 crystalline materials has been known for a long time [1–3]. In addition to experimental techniques providing some macroscopic physical quantities directly, like fluorine conductivity [4, 5], nuclear magnetic resonance (NMR) turned out to be very profitable in the investigations of the fluorine dynamics. Actually, the first indication of fast fluorine motion [1] arose from a motionally narrowed ^{19}F NMR spectrum detected for a LaF_3 crystal at room temperature. Such type of study can give a deep insight into the microscopic mechanism of the molecular dynamics, leading to the high conductivity. Important information about the local mechanism of the fluorine dynamics in lanthanum fluoride was already gained from an early NMR experiment [3]. The authors proved that there are at least two fluorine subsystems which exhibit fluorine dynamics on much different timescales. This result can be understood on the basis of the crystal structure of lanthanum

[3] Author to whom any correspondence should be addressed.

fluoride. It crystallizes in the tysonite structure ($P\bar{3}c1$) [6], which has three different fluorine sublattices called F_1, F_2 and F_3 with multiplicities of 12:4:2. The F_2 and the F_3 sublattices are dynamically very similar and can often be regarded as equivalent; therefore we will call the combined F_2–F_3 sublattice F_B and the F_1 sublattice F_A. The challenge, to link clearly and unambiguously the macroscopic properties of this relatively complex solid state system with its microscopic dynamics, has attracted broad attention for many years. Further NMR attempts to understand the motional mechanisms of the LaF_3 fluorine ions have been based on the fluorine lineshape [7, 8], gradient techniques [9] and relaxation analysis [10, 11], the last mentioned being especially valuable if performed over a broad frequency range using field cycling relaxometry [12]. Actually an answer to the long discussed question about the faster sublattice has been given on the background of the ^{19}F NMR lineshape measurements performed at high magnetic field [7, 8]. Two different fluorine subsystems have been clearly identified in the NMR spectrum by their chemical shifts; one of them corresponds to the crystallographic F_A sublattice, whereas the other one is formed by fluorine spins belonging to the F_B sublattice. Fast fluorine motion within the F_A sublattice leads to a narrowing of the corresponding resonance line. With increasing temperature the two lines, well separated at room temperature, overlap. This effect indicates thermally activated exchange motion between the two distinct sublattices. The lineshape study does not provide detailed information about temperature effects on the fluorine mobility inside the F_B sublattice, since the F_B line stays broad until it overlaps with the faster one. However, one can conclude, that the motion inside the F_B sublattice is so slow that it does not significantly affect the lineshape. These observations have been basically confirmed [13], by suppressing the dipolar line broadening in the NMR spectrum using magic angle spinning (MAS). This procedure made it possible to resolve the F_2 and the F_3 sublattices. It turned out that the F_3-ions are more mobile than the F_2-ions. A next step in the NMR investigations has been done in the direction of a quantitative description of the experimental lineshapes in terms of characteristic time constants reflecting the fluorine dynamics. This analysis ended up in the statement that it is necessary to assume a log-Gaussian distribution of the correlation times describing the motion within the F_A sublattice [14] as well as the F_A–F_B exchange process [15].

In the present work we return to the question about the fluorine dynamics in single crystals of lanthanum fluoride in much more detail, both experimentally and theoretically. Our current experimental results comprise NMR lineshape investigations for a series of $La_{1-x}Sr_xF_{3-x}$ single crystals with the systematically increasing concentration of admixtures: $x = 0$–16 mol%. This rich experimental data set reflects various aspects of the fluorine spin dynamics. For instance, the substitution of La^{3+} for Sr^{2+} does not change the tysonite structure for low concentrations, but it introduces fluorine vacancies into the lattice, which influence the fluorine dynamics. To extract the dynamic information an appropriate theoretical treatment is necessary. We propose in this paper a model describing the NMR spectrum in terms of three motional processes, namely the jump diffusion of the fluorine ions within the sublattices F_A and F_B, respectively, and the inter-lattice exchange motion. The surroundings of the particular spins representing the distinct sublattices are treated with caution. Here, all dipole–dipole couplings between equivalent as well as non-equivalent (belonging to different sublattices) fluorine spins, which are relevant for the NMR lineshape, are included into the theoretical description. Going beyond previous approaches, the present treatment also takes into account the effects of neighbouring lanthanum spins on the fluorine spectrum.

Let us anticipate one important conclusion. Principally, the results obtained by applying the current model to the experimental results confirm the outcome of the former studies [7, 8]. However, when taking into account all relevant dipole–dipole couplings, it turns out that one does not need to introduce the idea of heterogeneous fluorine motion represented by a

distribution of correlation times. The fluorine spectra can be reproduced by only two time constants, the first corresponding to the fast motion inside the F_A sublattice and the second describing the inter-lattice exchange motion.

This paper is organized as follows. Section 2 contains a description of experimental details, while the theoretical model is outlined in section 3. Section 4 covers relevant computational details, and an analysis of the experimental data and a discussion of the results are presented in sections 5 and 6, respectively. The last section contains concluding remarks.

2. Experimental details

Experimental NMR fluorine spectra have been collected for a pure LaF_3 single crystal and five crystals containing Sr^{2+} admixtures of concentrations of 0.01%, 0.03%, 1%, 3% and 16%. The relative accuracy of the concentrations has been estimated on the background of the crystal growing procedure as better than 30%. The experimental data for each sample consist of a series of 15–25 spectra, collected from room temperature up to 570–775 K. The upper temperature limit depends on the admixture concentrations and is given by the experimental linewidth approaching the resolution limit of the spectrometer (≈300 Hz). For the measurements single crystals of approximately $4 \times 4 \times 8$ mm^3 size were used. Their crystallographic orientation with respect to the c-axis was checked using Laue diffraction and polarization microscopy. The samples were sealed in quartz tubes under vacuum. Since the fluorine dynamics in a pure sample can change irreversibly after heating [9], the pure LaF_3 crystal was heated several times until no further ageing could be observed.

The ^{19}F NMR measurements were performed at 282 MHz using a TECMAG Apollo console on crystals orientated with their c-axis parallel to the magnetic field. The duration of a 90° pulse was 1.6 μs, the receiver dead time 2 μs. In spite of this finite dead time Fourier spectra of the free induction decay (FID) instead of echo signals were recorded. This choice is due to the fact that only the FID reproduces both chemical shift and dipole–dipole interactions simultaneously. To correct corrupted data points at the beginning of the FID signal a linear prediction algorithm [16] was applied to backward extrapolation of the recorded time signal. For the temperature adjustment a home-built probe head containing a micro furnace was used [17]. During acquisition the furnace was switched off to avoid any influences on the NMR signal. Since the acquisition takes at most a few milliseconds this has no influence on the temperature stability.

3. Theoretical description of the ^{19}F NMR lineshape in LaF_3

On the background of the experimental NMR spectra at room temperature one can distinguish two fluorine sublattices due to their chemical shifts. The sublattices, apart from being crystallographically distinct, also exhibit different fluorine dynamics. The first sublattice, denoted as F_A, is formed by the fluorine ions residing in the crystallographic positions F_1 of the LaF_3 crystal structure, while the second one, denoted as F_B, includes the fluorine ions located in the positions F_2 and F_3. Fluorine ions belonging to each of these sublattices, F_A and F_B, move among equivalent sites within the same sublattice and also jump to non-equivalent sites of the other sublattice. Fluorine spins are coupled by dipole–dipole interactions to neighbouring fluorine as well as lanthanum spins. The mutual dipole–dipole couplings affected by temperature-dependent jump dynamics of the fluorine ions determine the shape of the detected NMR spectra.

In this section we present the theoretical framework, which we shall apply later to analyse the experimental fluorine spectra.

For clarity of our description we consider first the isolated sublattice F_A, assuming that the internal fluorine dynamics is much faster than the inter-lattice exchange motion. In the next step we adapt our approach in a straightforward manner to the sublattice F_B. If the exchange processes between the two fluorine sublattices are slow compared to the motion of the fluorine ions within each of them, these sublattices can be treated separately. Finally we shall complete the description including exchange processes between the two fluorine subsystems.

In order to calculate the NMR spectrum for the F_A sublattice one needs to consider a group of spins, consisting of a reference spin I^A (treated as a representative of the F_A sublattice), and its surroundings, formed by N_A^A fluorine spins from the sublattice F_A, N_B^A spins from the sublattice F_B and N_{La}^A lanthanum spins. Thus, the selected spins form a system containing $N^A = N_A^A + 1 + N_B^A + N_{La}^A$ spins coupled by mutual dipole–dipole interactions. The total Hamiltonian H^A for the considered ensemble of spins contains the Zeeman couplings for the fluorine and lanthanum spins, and the dipolar interactions between all pairs of the spins:

$$H^A = \sum_{i=1}^{N_A^A+1} \omega_{F_A}(I_i^A)_z + \sum_{i=1}^{N_B^A} \omega_{F_B}(I_i^B)_z + \sum_{i=1}^{N_{La}^A} \omega_{La}(S_i)_z + H_{DD}^A. \tag{1}$$

The first two terms correspond to the Zeeman couplings of the fluorine spins belonging to the sublattices F_A and F_B, respectively. The Zeeman coupling of the reference fluorine spin I^A has been included into the first term. A chemical shift between the two fluorine groups $\sigma = |\omega_{F_A} - \omega_{F_B}|$ leads to the different resonance frequencies ω_{F_A} and ω_{F_B}. The third term describes the Zeeman couplings of the lanthanum spins included in the considered ensemble. The dipole–dipole Hamiltonian H_{DD}^A contains couplings between the reference spin I^A and particular spins from the environment, as well as dipole–dipole interactions between the environmental spins:

$$H_{DD}^A = \sum_{i,j=1\, i<j}^{N_A^A+1} l\ H_{DD}^{AA}(I_i, I_j) + \sum_{i=1}^{N_A^A+1}\sum_{j=1}^{N_B^A} H_{DD}^{AB}(I_i, I_j) + \sum_{i=1}^{N_A^A+1}\sum_{j=1}^{N_{La}^A} H_{DD}^{ALa}(I_i, S_j)$$
$$+ \sum_{i,j=1 i<j}^{N_B^A} H_{DD}^{BB}(I_i, I_j) + \sum_{i=1}^{N_B^A}\sum_{j=1}^{N_{La}^A} H_{DD}^{BLa}(I_i, S_j). \tag{2}$$

The first term describes mutual dipole–dipole interactions between the $(N_A^A + 1)$ spins from the F_A sublattice, including the spin I^A. The next two terms collect the couplings of the F_A spins to the N_B^A fluorine spins of the F_B group, and N_{La}^A lanthanum spins, respectively. Finally, the last two terms correspond to dipole–dipole couplings within the F_B sublattice and to the couplings between the F_B fluorine spins and the lanthanum spins, respectively. The dipole–dipole coupling between fluorine spins I_i and I_j, belonging to the F_α and F_β groups ($\alpha = A, B$; $\beta = A, B$), can be restricted in a high magnetic field to the zero-order term, and is given in the laboratory frame as [18, 19]

$$H_{DD}^{\alpha\beta}(I_i, I_j) = \frac{\mu_0}{4\pi}\frac{\gamma_F^2}{r_{I_iI_j}^3}\left(\frac{3\cos^2\theta_{I_iI_j,L} - 1}{2}\right)\left[2I_{iz}I_{jz} - \frac{1}{2}(I_{i+}I_{j-} + I_{i-}I_{j+})\right]. \tag{3}$$

The angle $\theta_{I_iI_j,L}$ describes the orientation of the $I_i - I_j$ dipole–dipole axis with respect to the laboratory frame, while $r_{I_iI_j}$ is the inter-spin distance. For non-equivalent spins like fluorine and lanthanum, the high-field dipole–dipole coupling can be simplified even more by neglecting

the flip-flop terms:

$$H_{\mathrm{DD}}^{\alpha\mathrm{La}}(I_i, S_j) = \frac{\mu_0}{4\pi}\frac{\gamma_{\mathrm{F}}\gamma_{\mathrm{La}}}{r^3_{I_i S_j}}\left(\frac{3\cos^2\theta_{I_i S_j,L} - 1}{2}\right)[2I_{iz}S_{jz}]. \tag{4}$$

The Hamiltonian H^A determines the energy levels of the selected system of coupled spins. To obtain the required eigenvalues we diagonalize the Hamiltonian H^A in the Zeeman basis $|n\rangle = |m_1^A, \ldots, m^A_{N_A^A+1}, m_1^B, \ldots, m^B_{N_B^A}, m_1^{\mathrm{La}}, \ldots, m^{\mathrm{La}}_{N_{\mathrm{La}}^A}\rangle$. The particular magnetic quantum numbers m_i^A, m_i^B and m_i^{La}, correspond to the fluorine spins from the sublattices $\mathrm{F}_A, \mathrm{F}_B$ and the lanthanum spins, respectively. The numbers of the spins included into the considerations determines the number of the energy levels for the system: $(2I_{\mathrm{F}}+1)^{N_A^A+1+N_B^A}(2S_{\mathrm{La}}+1)^{N^a_{\mathrm{La}}}$, where $I_{\mathrm{F}} = \frac{1}{2}$, $S_{\mathrm{La}} = \frac{7}{2}$. Single-quantum transitions of the reference fluorine spin I^A, being a part of the coupled spin system, give rise to the observed spectrum of the F_A sublattice. The relevant transition frequencies include the main resonance frequency ω_{F_A} affected by the dipole–dipole couplings and can be selected from all transition frequencies $\omega^A_{\alpha\alpha'} = E^A_\alpha - E^A_{\alpha'}$ between the energy levels, E^A_α, of the considered spin system. In the further considerations we denote the particular single-quantum coherences as ω^A_μ, i.e. μ replaces the pairs of indices $\alpha\alpha'$ in the frequencies associated with single-quantum transitions of the spin I^A. We also denote the number of relevant single-quantum transitions of the spin I^A by N^A_{SQ}, thus $\mu = 1, \ldots N^A_{\mathrm{SQ}}$. The effects of the jump of the fluorine spin I^A from one site of the sublattice F_A to another can be treated as a change of its frequency ω^A_μ caused by different quantum configuration of the new surroundings. On this background one can set up an equation of motion for the density operator $\sigma_A(t)$, describing the selected spin system, in the form

$$\frac{\mathrm{d}\sigma^A_\mu(t)}{\mathrm{d}t} = -\mathrm{i}\omega^A_\mu\sigma^A_\mu(t) + \sum_\nu \Gamma^A_{\mu\nu}\sigma^A_\nu(t) = \sum_\nu(-\mathrm{i}\omega^A_\nu\delta_{\nu\mu} + \Gamma^A_{\mu\nu})\sigma^A_\nu(t) = \sum_\nu A_{\mu\nu}\sigma^A_\nu(t). \tag{5}$$

The summation is restricted to the single-quantum coherences relevant for the F_A fluorine spectrum. In the last equality we introduce the matrix A defined as $A_{\mu\nu} = -\mathrm{i}\omega^A_\nu\delta_{\nu\mu} + \Gamma^A_{\mu\nu}$. The elements $\Gamma^A_{\mu\nu}$ are determined by the lifetime, τ_{AA}, for the fluorine spins from the sublattice F_A to stay at a certain position.

The time-domain NMR signal for a spin I is given by the trace of the product of an appropriate density operator $\sigma(t)$ and the operator I_-. Thus, the F_A lineshape $S_{\mathrm{F}_A}(\omega)$ can be obtained, as a Fourier transform of the corresponding time-domain signal, from the following expression [19]:

$$S_{\mathrm{F}_A}(\omega) \cong \int_0^\infty \mathrm{Tr}\{\sigma_A(t)I^A_-\}\exp(-\mathrm{i}\omega t)\,\mathrm{d}t \cong W\cdot(A - \mathrm{i}\omega 1)^{-1}\cdot 1 \cong \sum_{\mu\nu}[(A-\mathrm{i}\omega 1)^{-1}]_{\mu\nu}. \tag{6}$$

The vector W contains the initial density matrix elements $W_\nu = \sigma_\nu(0)$ proportional to probabilities of the corresponding coherences ω_ν. Since the probabilities are equal they are omitted in the last part of equation (6). To complete the expression for the F_A fluorine spectrum one needs to define the transition rates $\Gamma^A_{\mu\nu}$. The jump rate of the fluorine spin I^A from one F_A position to another F_A position is defined as the inverse lifetime τ^{-1}_{AA}. Performing such a jump, the spin I^A changes its transition frequency from a value ω^A_μ (experienced in the initial position) to one of the possible values ω^A_ν ($\nu = 1, \ldots, N^A_{\mathrm{SQ}}$) associated with the actual new site. In particular, if $\omega^A_\mu = \omega^A_\nu$ the spin does not notice anything. This implies that a jump of the spin I^A among two frequency values ω^A_μ and $\omega^A_\nu (\mu \neq \nu)$ occurs with the rate $\Gamma^A_{\mu\nu} = \Gamma^A_{\nu\mu} = (N^A_{\mathrm{SQ}}\tau_{AA})^{-1}$. The diagonal elements $\Gamma^A_{\mu\mu}$ correspond to the jump rate from the

frequency ω_μ^A to one of the $(N_{\mathrm{SQ}}^A - 1)$ others and are given as $\Gamma_{\mu\mu}^A = -(N_{\mathrm{SQ}}^A - 1)(N_{\mathrm{SQ}}^A \tau_{AA})^{-1}$. Linking the transition rates $\Gamma_{\mu\nu}^A$ to the lifetime τ_{AA}, we have completed equation (6) describing the theoretical lineshape of the F_A fluorine spins, under the assumption that the fluorine spins do not leave their sublattice.

The lineshape description can easily be adapted to the F_B sublattice. First, we need to choose the appropriate surroundings of a reference spin I^B (representing the sublattice F_B). Assuming that its environment consists of N_A^B fluorine spins from the sublattice F_A, N_B^B spins from the sublattice F_B and N_{La}^B lanthanum spins, one needs to calculate the set of possible frequencies ω_μ^B for single-quantum transitions of the spin I^B. Knowing the relevant transition frequencies, the equation of motion for the density operator $\sigma_B(t)$ can be set up in full analogy to equation (5): $\frac{\mathrm{d}\sigma_\mu^B(t)}{\mathrm{d}t} = \sum_\nu B_{\mu\nu}\sigma_\nu^B(t)$. The matrix B is now defined as $B_{\mu\nu} = -\mathrm{i}\omega_\nu^B\delta_{\nu\mu} + \Gamma_{\mu\nu}^B$, with the off-diagonal elements $\Gamma_{\mu\nu}^B = \Gamma_{\nu\mu}^B = (N_{\mathrm{SQ}}^B\tau_{BB})^{-1}$, while $\Gamma_{\mu\mu}^B = -(N_{\mathrm{SQ}}^B - 1)(N_{\mathrm{SQ}}^B\tau_{BB})^{-1}$. The number of frequencies for single-quantum transitions of the spin I^B, generated by its surroundings, is denoted as N_{SQ}^B, while τ_{BB} is the lifetime for the F_B fluorine ions. The expression $S_{\mathrm{F}_B}(\omega) \cong \sum_{\mu\nu}[(B - \mathrm{i}\omega 1)^{-1}]_{\mu\nu}$ gives the theoretical NMR spectrum for the F_B sublattice.

At this point, before we complete the approach introducing exchange effects, some comments concerning the choice of the environmental spins are appropriate. Choosing the environment of the reference spins I^A and I^B, one has to look for a compromise between the computational complexity (caused by the number of included spins) and a significance of effects caused by including more spins into the considered surroundings. The ranking of spins included into the surroundings is established by the dipole–dipole splitting (equations (3) and (4)), determined by the inter-spin distance, the orientation of the dipole–dipole axis with respect to the laboratory frame and the gyromagnetic ratio as well as the spin quantum number.

If exchange processes between the sublattices contribute effectively to the dynamics of the fluorine ions, the two sublattices cannot be treated anymore as dynamically isolated. To evaluate the fluorine spectrum one needs to set up a common dynamic matrix including the matrices A and B for the particular sublattices F_A and F_B, modified now by the exchange dynamics and coupled by appropriate exchange terms. Let us discuss the inter-lattice exchange effects from the point of view of the sublattice F_A represented by the spin I^A. The opportunity to jump from the F_A sublattice to a non-equivalent position in the sublattice F_B increases the number of single-quantum transition frequencies available for the I^A spin. Thereby its transition frequency can change from the initial value ω_μ^A to one of the frequencies ω_ν^A ($\nu = 1, \ldots, N_{\mathrm{SQ}}^A$) characteristic for the F_A sublattice with the ratio $\Gamma_{\mu\nu}^A = \Gamma_{\nu\mu}^A = (N_{\mathrm{SQ}}^A\tau_{AA})^{-1}$ or to one of the frequencies ω_ν^B ($\nu = 1, \ldots, N_{\mathrm{SQ}}^B$) characterizing the F_B sites. The jump $\omega_\mu^A \to \omega_\nu^B$ occurs with the ratio $\Gamma_{\mu\nu}^{AB} = (N_{\mathrm{SQ}}^B\tau_{AB})^{-1}$ where τ_{AB}^{-1} denotes the jump rate from a F_A site to the sublattice F_B. The exchange degrees of freedom lead to a common dynamic matrix Λ including the matrices A and B with their sets of frequencies ω_ν^A and ω_ν^B, as well as the inter-lattice exchange rates. The dimension of the matrix Λ is given by the sum of the considered single-quantum transitions of fluorine spins from both sublattices: $N = N_{\mathrm{SQ}}^A + N_{\mathrm{SQ}}^B$ (i.e. the dimension of the matrix Λ is given by the sum of the dimensions of the matrices A and B). The diagonal elements of the matrix Λ take the form

$$\Lambda_{\mu\mu} = -\mathrm{i}\omega_\mu^A - (N_{\mathrm{SQ}}^A - 1)(N_{\mathrm{SQ}}^A\tau_{AA})^{-1} - \tau_{AB}^{-1}, \qquad 1 \leqslant \mu \leqslant N_{\mathrm{SQ}}^A \tag{7}$$

$$\Lambda_{\mu\mu} = -\mathrm{i}\omega_\mu^B - (N_{\mathrm{SQ}}^B - 1)(N_{\mathrm{SQ}}^B\tau_{BB})^{-1} - \tau_{BA}^{-1}, \qquad N_{\mathrm{SQ}}^A < \mu \leqslant N_{\mathrm{SQ}}^A + N_{\mathrm{SQ}}^B. \tag{8}$$

The exchange lifetime τ_{BA} is related to τ_{AB} by the ratio between the numbers of spins $(n_{\mathrm{F}_A}, n_{\mathrm{F}_B})$ forming the particular sublattices: $\tau_{AB} = \frac{n_{\mathrm{F}_A}}{n_{\mathrm{F}_B}}\tau_{BA}$ (i.e. $\tau_{AB} = 2\tau_{BA}$). The exchange

rates τ_{AB}^{-1} and τ_{BA}^{-1}, added to the diagonal elements of the matrix Λ, reflect the exchange degrees of freedom of the spins I^A and I^B, which can move between the sublattices. Off-diagonal elements of the matrix Λ, which correspond to off-diagonal parts of the isolated matrices A and B, remain unchanged:

$$\Lambda_{\mu\nu} = (N_{\mathrm{SQ}}^A \tau_{AA})^{-1}, \qquad 1 \leqslant \mu, \nu \leqslant N_{\mathrm{SQ}}^A, \qquad \mu \neq \nu \tag{9}$$

$$\Lambda_{\mu\nu} = (N_{\mathrm{SQ}}^B \tau_{AA})^{-1}, \qquad N_{\mathrm{SQ}}^A < \mu, \nu \leqslant N_{\mathrm{SQ}}^A + N_{\mathrm{SQ}}^B, \qquad \mu \neq \nu. \tag{10}$$

Finally, the matrix Λ has to be completed by the elements providing the 'exchange link' between the sublattices F_A and F_B:

$$\Lambda_{\mu\nu} = (N_{\mathrm{SQ}}^B \tau_{AB})^{-1}, \qquad 1 \leqslant \mu \leqslant N_{\mathrm{SQ}}^A, \qquad N_{\mathrm{SQ}}^A < \nu \leqslant N_{\mathrm{SQ}}^A + N_{\mathrm{SQ}}^B \tag{11}$$

$$\Lambda_{\mu\nu} = (N_{\mathrm{SQ}}^A \tau_{BA})^{-1}, \qquad N_{\mathrm{SQ}}^A < \mu \leqslant N_{\mathrm{SQ}}^A + N_{\mathrm{SQ}}^B, \qquad 1 \leqslant \nu \leqslant N_{\mathrm{SQ}}^A. \tag{12}$$

The theoretical lineshape $S_{\mathrm{F}}(\omega)$ for both the fluorine sublattices including exchange effects between them can be described by

$$S_{\mathrm{F}}(\omega) \cong \sum_{\mu\nu} W_\nu [(\Lambda - \mathrm{i}\omega 1)^{-1}]_{\mu\nu} \tag{13}$$

where the population matrix W reflects the ratio between the number of spins $n_{\mathrm{F}_A}, n_{\mathrm{F}_B}$, i.e. $W_\nu = 1$ for $1 \leqslant \nu \leqslant N_{\mathrm{SQ}}^A$, and $W_\nu = \frac{n_{\mathrm{F}_B}}{n_{\mathrm{F}_A}} = \frac{1}{2}$ for $N_{\mathrm{SQ}}^A < \nu \leqslant N_{\mathrm{SQ}}^A + N_{\mathrm{SQ}}^B$. The final structure of the matrix $(\Lambda - \mathrm{i}\omega 1)$ is presented in diagram 1.

4. Structural and computational details

The tysonite $P\bar{3}c1$ structure of LaF_3 is determined by two lattice constants $a = b = 7.185$ Å and $c = 7.351$ Å (at $T = 295$ K), and two angles $\alpha = \beta = 90°$ and $\gamma = 120°$ [20]. The unit cell contains 12 fluorine spins forming the F_1 sublattice. They positions expressed in terms of the lattice coordinates $x = 0.366$, $y = 0.054$ and $z = 0.081$ are as follows: $(\pm x, \pm y, \pm z)$, $(\pm y, \pm(y-x), \mp z)$, $(\pm(x-y), \pm x, \mp z)$, $(\pm y, \pm x, \mp(z+0.5))$, $(\pm x, \pm(x-y), \mp(z+0.5))$ and $(\pm(y-x), \pm y, \pm(z+0.5))$. The F_2 sublattice is represented within the unit cell by four ions at the positions $(\pm 1/3, \pm 2/3, \pm z)$, $(\pm 1/3, \pm 2/3, \pm z \pm 0.5)$, where $z = 0.187$, while the F_3 sublattice covers two ions: $(0, 0, \pm 1/4)$. The lanthanum ions occupy six positions within the unit cell: $(\pm x, 0, \pm 1/4)$, $(0, \pm x, \pm 1/4)$ and $(\pm x, \pm x, \mp 1/4)$. On this structural background we have set up the ensemble of fluorine and lanthanum spins forming the surroundings of the reference F_A and F_B fluorine ions, included into the calculations. The participating spins have been selected from the group covering all crystallographic positions labelled by the Miller indices h, k, l ranging over 0 and ± 1. Taking into account the strength of the dipole–dipole interactions (equations (3) and (4)) we have involved in the calculations of the F_A line eight fluorine spins ($N_A^A = 7$, $N_A^B = 1$) and one lanthanum spin ($N_A^{\mathrm{La}} = 1$). The F_B line has been calculated for five most important neighbours ($N_B^A = 3$, $N_B^B = 2$, $N_B^{\mathrm{La}} = 0$). We have tested this computational treatment by including more spins into the F_A as well as F_B group. We have found out that the additional spins do not influence the calculated spectra on a noticeable level. We have not considered eventual temperature and doping effects on the structure parameters.

5. Analysis of the experimental NMR lines

Within the framework of the presented model we have analysed six series of experimental NMR spectra ($x = 0\%$, 0.01%, 0.03%, 1%, 3% and 16%). To explain the strategy of the analysis we start from general comments appropriate for all the investigated crystals. The room-temperature

$\Lambda - \mathrm{i}\omega 1 =$

$-\mathrm{i}(\omega+\omega_1^A)$ $-\Gamma^A-\tau_{AB}^{-1}$	$(N_{\mathrm{SQ}}^A\tau_{AA})^{-1}$	$(N_{\mathrm{SQ}}^A\tau_{AA})^{-1}$	$(N_{\mathrm{SQ}}^B\tau_{AB})^{-1}$	$\ldots$	$(N_{\mathrm{SQ}}^B\tau_{AB})^{-1}$
$(N_{\mathrm{SQ}}^A\tau_{AA})^{-1}$	$-\mathrm{i}(\omega+\omega_i^A)$ $-\Gamma^A-\tau_{AB}^{-1}$	$(N_{\mathrm{SQ}}^A\tau_{AA})^{-1}$	$\ldots$	$\ldots$	$\ldots$
$(N_{\mathrm{SQ}}^A\tau_{AA})^{-1}$	$(N_{\mathrm{SQ}}^A\tau_{AA})^{-1}$	$-\mathrm{i}(\omega+\omega_{N_{\mathrm{SQ}}^A}^A)$ $-\Gamma^A-\tau_{AB}^{-1}$	$(N_{\mathrm{SQ}}^B\tau_{AB})^{-1}$	$\ldots$	$(N_{\mathrm{SQ}}^B\tau_{AB})^{-1}$
$(N_{\mathrm{SQ}}^A\tau_{BA})^{-1}$	$\ldots$	$(N_{\mathrm{SQ}}^A\tau_{BA})^{-1}$	$-\mathrm{i}(\omega+\omega_1^B)$ $-\Gamma^B-\tau_{BA}^{-1}$	$(N_{\mathrm{SQ}}^B\tau_{BB})^{-1}$	$(N_{\mathrm{SQ}}^B\tau_{BB})^{-1}$
$\ldots$	$\ldots$	$\ldots$	$(N_{\mathrm{SQ}}^B\tau_{BB})^{-1}$	$-\mathrm{i}(\omega+\omega_j^B)$ $-\Gamma^B-\tau_{BA}^{-1}$	$(N_{\mathrm{SQ}}^B\tau_{BB})^{-1}$
$(N_{\mathrm{SQ}}^A\tau_{BA})^{-1}$	$\ldots$	$(N_{\mathrm{SQ}}^A\tau_{BA})^{-1}$	$(N_{\mathrm{SQ}}^B\tau_{BB})^{-1}$	$(N_{\mathrm{SQ}}^B\tau_{BB})^{-1}$	$-\mathrm{i}(\omega+\omega_{N_{\mathrm{SQ}}^B}^B)$ $-\Gamma^B-\tau_{BA}^{-1}$

Diagram 1. Structure of the evolution (exchange) matrix, $\Lambda - \mathrm{i}\omega 1$, including the dynamic processes within the particular sublattices as well as the exchange motion between them. The block corresponding to the F_A sublattice is numbered by indices k, l in the range $1 < k, l < N_{\mathrm{SQ}}^A$, while the block with $N_{\mathrm{SQ}}^A < k, l < N_{\mathrm{SQ}}^A + N_{\mathrm{SQ}}^B$ corresponds to the F_B sublattice. The indices i and j denote individual single-quantum transitions of the F_A and F_B spins, respectively; $1 < i < N_{\mathrm{SQ}}^A, 1 < j < N_{\mathrm{SQ}}^B$. The remaining matrix elements reflect the exchange dynamics between the two sublattices.

spectra always consist of two well resolved lines corresponding to the F_A and F_B sublattices, with chemical shifts of $\sigma = 163$–170 ppm. An example of such a spectrum is presented in figure 1 (spectrum (a)), $x = 0.3\%$, $T = 295$ K. One can conclude from the room-temperature spectra, characterized for all samples by a broad F_B line, that the fluorine motion inside the combined F_B sublattice is much slower than the motion inside the F_A sublattice. In the analysis we set the lifetime of the F_B spins to $\tau_{BB} = 1.6 \times 10^{-4}$ s. The theoretical curve obtained for this τ_{BB} value reproduces the shape of the F_B part of the NMR spectra well, as shown in figure 1. It is important to note that the τ_{BB} time value reflects only the fact that the motion inside the F_B is relatively slow and one should not treat it as a precise characterization of this process. The experimental spectra do not carry accurate information about dynamic processes, if they become significantly slower than the experimental time-window determined by the duration of the detected FID.

Since there is no evidence for exchange processes between the two sublattices F_A and F_B at room temperature, we reproduce the spectra without including the exchange dynamics into the analysis. Nevertheless, the observed symmetrical lines can also be reproduced by assuming an exchange lifetime of the order of milliseconds, since both lines of the spectra are still symmetrical for exchange processes occurring on this timescale. Such a treatment would alter the corresponding value for τ_{AA} only marginally. At higher temperatures the exchange lifetime is unambiguously determined by the lineshape.

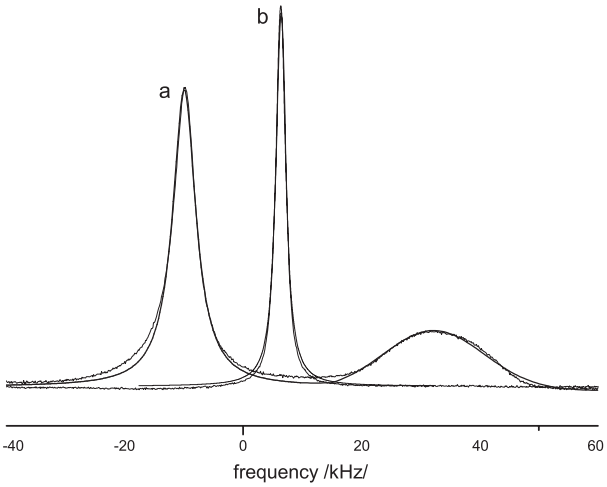

Figure 1. Experimental and calculated fluorine NMR spectra for a LaF_3 single crystal containing 0.3% Sr^{2+} admixtures. Spectra (a) and (b) were collected for the temperatures $T = 295$ and 700 K. The corresponding theoretical curves, shown as solid lines, are obtained for $\tau_{AA} = 4.0 \times 10^{-6}$ s (a) and $\tau_{AA} = 1.0 \times 10^{-8}$ s, $\tau_{BA} = 5.9 \times 10^{-7}$ s (b).

The chemical shift is treated as a constant parameter for the whole data set of a given concentration x and it is equal to the room-temperature value. When the temperature increases the τ_{AA} and τ_{BA} processes become faster. Interplay between them leads to a progressing overlap of the F_A and F_B lines, which were well resolved at room temperature. Therefore, the spectra take up a form of one, initially strongly asymmetrical, line. A further temperature increase reduces the asymmetry and the line becomes continuously narrower, reaching finally the resolution limit (spectrum (b) in figure 1). In this temperature regime the lineshape is fully determined by the exchange processes encoded in the correlation time τ_{BA}, and the NMR spectra do not provide any more information about the fast fluorine dynamics inside the F_A sublattice. Since the jump diffusion within the F_B sublattice occurs on much slower timescale than for the F_A ions, the lineshape of the F_B sublattice is dominated in the whole temperature range by the exchange processes (τ_{BA}).

To illustrate the temperature changes of the NMR spectra we present in figure 2 a set of experimental data for the pure crystal. The figure covers the most interesting temperature range, where one observes the successive transition from two-line to one-line spectra. The theoretical curves corresponding to the lower temperatures of this range are still modelled by both dynamic processes (τ_{AA} and τ_{BA}). However, the effect of the τ_{AA} lifetime on the lineshapes continuously diminishes and therefore the higher-temperature spectra are modelled mainly by the exchange lifetime τ_{BA}. More experimental and calculated lineshapes for the other crystals ($x = 0.01\%$, 0.3%, 1%, 3%, 16%) are presented in the appendix in figures A.1–A.5.

Finally, some comments on the level of agreement between the experimental data and the fitted theoretical lines are appropriate. As can be seen in figures 1, 2 and A.1–A.4 there are some minor deviations of the theoretical curves from the experimental ones, especially on the wings of the spectra. Since the experimental spectra were obtained from the corresponding FID signals following a 90° pulse, they suffer from dead time effects. There are two important consequences of the finite dead time. First, the spectra require additional phase and baseline corrections, which obviously affect the lineshape. Furthermore, information which is encoded in the first points of the FID is unavoidably lost. To reduce the dead time effect by backward

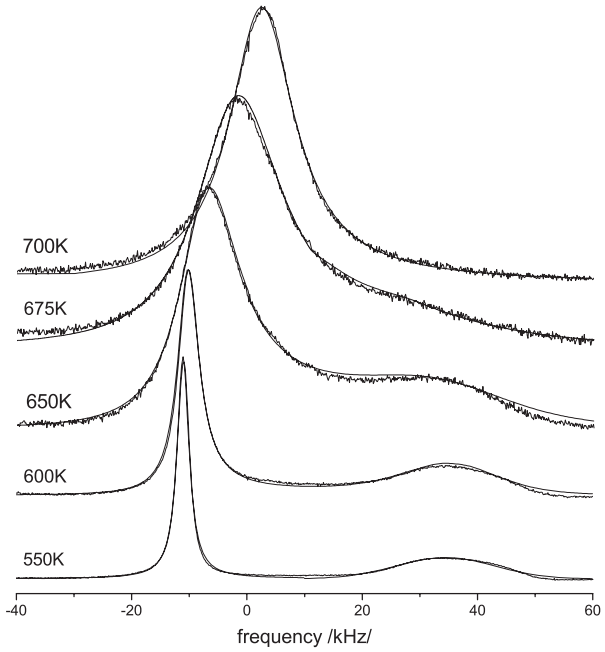

Figure 2. Experimental fluorine spectra for a pure LaF_3 crystal in the temperature range 550–700 K, together with lines calculated for the parameter values obtained from least square fitts. The effect of the τ_{AA} parameter on the lineshape diminishes continuously with increasing temperature. For higher temperatures the spectra are modelled merely by the inter-lattice exchange τ_{BA}. 550 K: $\tau_{AA} = 8.0 \times 10^{-7}$ s, $\tau_{BA} = 1.6 \times 10^{-4}$ s; 600 K: $\tau_{AA} = 1.6 \times 10^{-7}$ s, $\tau_{BA} = 3.7 \times 10^{-5}$ s; 650 K: $\tau_{BA} = 1.3 \times 10^{-5}$ s; 675 K: $\tau_{BA} = 4.9 \times 10^{-6}$ s; 700 K: $\tau_{BA} = 3.1 \times 10^{-6}$ s.

extrapolation, we used a linear prediction algorithm on the measured FID signal. This treatment avoided the baseline corrections and significantly reduced the discrepancies between the experiment and the theoretical lineshapes. Nevertheless, it should be realized that the linear prediction method gives us only an estimation of the initial data points.

6. Discussion

The resulting lifetimes τ_{AA} and τ_{BA}, describing the dynamics of the F_A fluorine ions within their own sublattice and the exchange processes between the two distinct sublattices F_A and F_B are collected in figures 3–5 for various concentrations of the admixtures.

In figure 3 we include a few representative error bars illustrating the two effects mentioned in section 4. The relatively large fitting error of the exchange lifetime τ_{BA} as well as of τ_{AA} at $T = 500$ K reflects the discussed uncertainty of the exchange effects at relatively low temperatures. The decreasing influence of the τ_{AA} parameter on the lineshapes is reflected by the corresponding τ_{AA} error bars, which become much larger at higher temperatures, where the lineshape is mainly dominated by the exchange motion. This behaviour of the fitting errors is common for all analysed crystals. The error bars of the other data points are smaller (5–15%), therefore we do not present them.

The temperature dependence of most of the processes can be described by an Arrhenius law, $\ln(\tau_c) \propto T^{-1}$, although some deviations occur. The most pronounced deviations from the Arrhenius behaviour can be observed for the time constant τ_{AA} of the pure sample, where

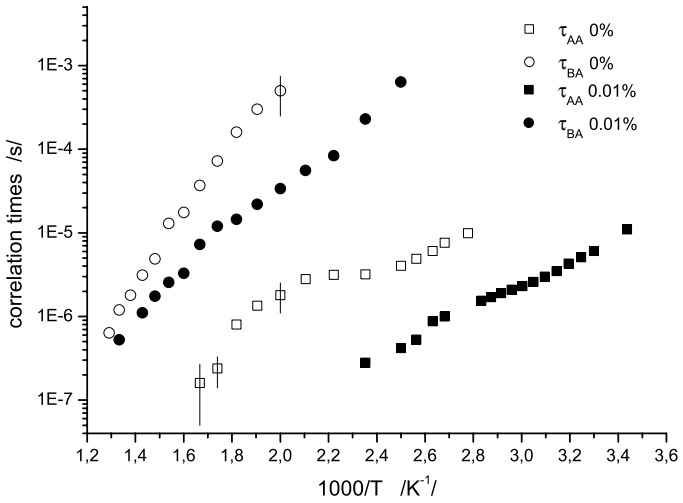

Figure 3. Temperature dependences of the τ_{AA} and τ_{BA} time constants for a pure LaF_3 crystal as well as a crystal containing 0.01% admixtures. The error bars refer to the discussion in the text.

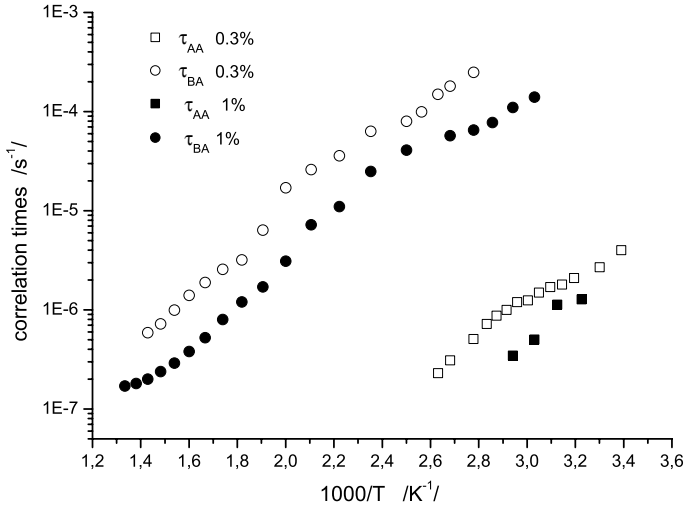

Figure 4. Temperature dependences of the parameters τ_{AA} and τ_{BA} for LaF_3 crystals with the concentrations of admixtures $x = 0.3\%$ and $x = 1\%$.

a significant change of the slope can be seen. This may suggest three temperature regimes of different activation energies for the jump diffusion inside the F_A sublattice, but due to the small number of data points and the increasing error at high temperatures (cf figure 3) no reliable statement can be formulated. Three different slopes have already been reported for conductivity measurements of pure and Ba^{2+}-doped LaF_3 [4]. Less pronounced deviations from a simple Arrhenius behaviour can be observed for the exchange lifetime τ_{BA} of the $x = 1\%$ and 3% samples. Here the low- and high-temperature data points seem to follow the same temperature dependence, whereas there is an evidence of slightly longer exchange correlation times in the intermediate temperature range. We are aware that statements about a non-Arrhenius dynamics of the fluorine spins must be better motivated by independent measurements. Nevertheless,

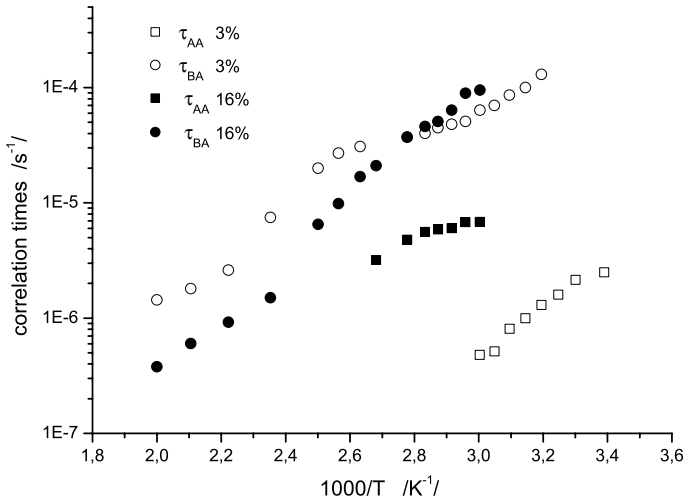

Figure 5. Temperature dependences of the parameters τ_{AA} and τ_{BA} for LaF_3 crystals with the concentrations of admixtures $x = 3\%$ and 16%.

except for τ_{AA} of the pure sample, all measurements can reasonably be approximated in the observed temperature range by an Arrhenius law.

As can be seen in figures 3–5, exchange processes between the distinct sublattices are about two orders of magnitude slower than the motion within the F_A sublattice, except for the 16% sample. Comparing the temperature dependence of both processes one observes that for low admixture concentrations the slope of the exchange lifetime τ_{BA} is larger than that of τ_{AA}. As a consequence the time constants of both processes get closer at higher temperatures and they may even merge or cross. For higher concentrations of admixtures ($x = 1\%$ as well as $x = 3\%$) both processes exhibit similar activation energies, hence the τ_{AA} and τ_{BA} curves are parallel. However, for $x = 16\%$ the difference of the slopes becomes visible again and the τ_{AA} and τ_{BA} have the tendency to merge within the observed temperature range.

Comparing the results for τ_{AA} for the differently doped samples it is apparent that the motion within the F_A sublattice gets faster with increasing dopant concentration up to $x = 1\%$. The dynamics within the F_A sublattice for $x = 3\%$ turns out to be very similar to $x = 1\%$, whereas the $x = 16\%$ sample shows significantly longer time constants. This observation is consistent with conductivity measurements on Sr^{2+}-doped LaF_3, where also a decrease of the conductivity for concentrations above $x \approx 3\%$ between 300 and 400 K is reported [4].

Analogously, with increasing admixture concentration the exchange process gets faster in the observed temperature range.

Let us discuss the fluorine dynamics also in terms of activation energies E_A and E_{BA}. The activation energy for the diffusion inside the F_A sublattice, E_A, increases with dopant concentration from (0.28 ± 0.03) eV for $x = 0.01\%$ to (0.40 ± 0.04) eV for $x = 3\%$, at the same time as the activation energy of the inter-lattice exchange, E_{BA}, decreases systematically from (0.82 ± 0.03) eV for the pure sample to (0.33 ± 0.02) eV for $x = 3\%$. Both trends break down for the sample with the highest concentration, $x = 16\%$, characterized by $E_A = (0.20 \pm 0.05)$ eV, and $E_{BA} = (0.52 \pm 0.03)$ eV.

The analysis of the highly doped sample is based on the crystallographic data of pure LaF_3. Although the tysonite structure is kept for samples with $x = 16\%$, one can expect that the structure gets significantly deformed by the admixtures. Thus, one has to be aware that the results for highly doped samples are affected by structural modifications.

Finishing the discussion, we wish to point out that the theoretical analysis is based on two parameters only, the time constants τ_{AA}, τ_{BA}, without any distribution of them. In former studies [12, 14, 15] it had been necessary to assume log-Gaussian distributions of the correlation times to get an acceptable agreement between the calculations and the experiment. The discrepancies between the previous studies and the current one require some comments. The fluorine relaxation data presented in [12] were based on the BPP (Bloembergen–Purcell–Pound) [21, 9] expression, which is appropriate for systems of identical spins $1/2$, coupled by dipole–dipole interactions. Since LaF_3 contains two distinct fluorine sublattices and quadrupole spins, a more advanced theoretical treatment is necessary to interpret the relaxation data. We have developed for this purpose a proper relaxation model, which is a complicated subject by itself and to which we shall devote forthcoming papers. We have found out that the relaxation data collected for the same LaF_3 crystals can also be interpreted satisfactorily and consistently in terms of single correlation times.

The lineshape analysis presented in [14] had been carried out within a simplified theoretical approach. The spectra had been calculated for a reference fluorine spin including its dipole–dipole interactions with up to eight surrounding fluorines. The contribution of the lanthanum spins had been neglected. In this paper we deal with the whole ensemble of the selected spins including *all* interactions between them. One should realize that the present approach requires working with large matrices, which, due to limited computer power, was problematic a couple of years ago.

We do not intend to claim that the lattice dynamics in this rather complex system is just homogenous and fully described by the two correlation times. However, the lineshape data can satisfactorily be explained within the present motional model.

7. Concluding remarks

We have developed a model for the fluorine NMR lineshape for the LaF_3 crystal structure based on the concept of three motional processes characterized by well defined correlation times. The model includes jump diffusion of the fluorine ions among equivalent sites within two crystallographically distinct sublattices, and inter-lattice exchange processes. The theoretical description has been based on a detailed treatment of fluorine–fluorine and fluorine–lanthanum dipole–dipole interactions relevant for the shape of the fluorine spectra. We have applied the model to experimental lineshape data collected for a series of LaF_3 single crystals with systematically increasing concentration of admixtures: $La_{1-x}Sr_xF_{3-x}$ crystals ($x = 0$–16%) from room temperature up to 775 K. This theoretical approach leads to a satisfactory interpretation of the NMR data, without involving any additional parameters associated with motional heterogeneities like a distribution of correlation times. We have discussed the temperature dependences of the time constants describing the fast fluorine ion motion inside one of the sublattices as well as the exchange processes.

Acknowledgment

This work was supported by the Deutsche Forschungsgemeinschaft (DFG) under grant no. FU 308/4.

Appendix

Figure A.1 illustrates the temperature changes of the NMR spectra for the doped material with $x = 0.01\%$. The lineshapes are determined by the inter-lattice exchange (τ_{BA}). To reproduce them it is enough to assume that τ_{AA} is at least of the order of 10^{-7} s.

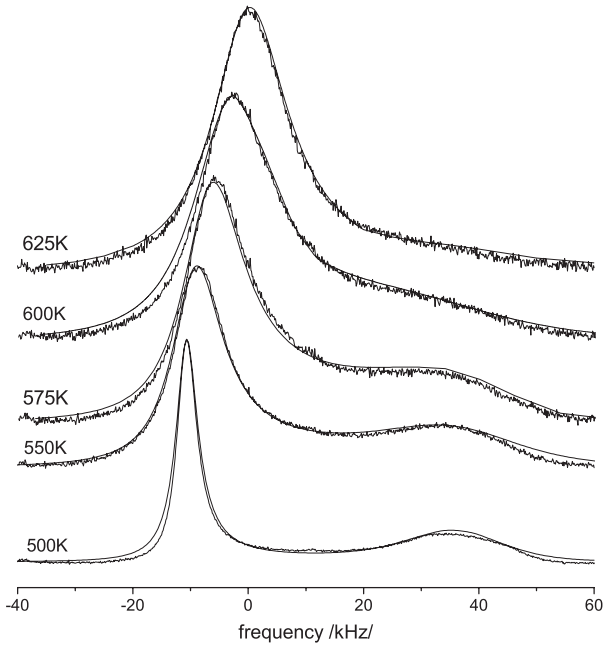

Figure A.1. Experimental and calculated fluorine spectra for a LaF_3 crystal containing 0.01% Sr^{2+} admixtures in the temperature range 500–625 K. The exchange lifetime τ_{BA} values are as follows. 500 K: $\tau_{BA} = 3.4 \times 10^{-5}$ s; 550 K: $\tau_{BA} = 1.45 \times 10^{-5}$ s; 575 K: $\tau_{BA} = 1.2 \times 10^{-5}$ s; 600 K: $\tau_{BA} = 7.3 \times 10^{-6}$ s; 625 K: $\tau_{BA} = 3.3 \times 10^{-6}$ s.

In figure A.2 we show some fluorine spectra of the crystal containing 0.3% admixtures, selected from the temperature range 450–575 K. The spectrum at $T = 450$ K is quite similar to the spectrum obtained for the crystal with the lower concentration of admixtures $x = 0.01\%$ at the temperature $T = 500$ K, and already determined in principle by the exchange process τ_{BA}.

Figure A.3 presents some examples of fluorine spectra collected for the crystal with 1% of the admixtures. The spectrum at $T = 310$ K can be reproduced neglecting the inter-lattice exchange. The F_A line of the next spectrum, for $T = 360$ K, is broader compared to the case of $T = 310$ K, and shifted to the right. The effects prove that for the higher temperature the exchange motion is significantly faster than for the lower one. Actually the spectrum for $T = 360$ K is determined only by the exchange process being fast enough to mask the influence of the τ_{AA} motion. This effect starts even earlier, at $T = 350$ K (the spectrum is not shown). The higher-temperature spectra reflect the progressively faster inter-lattice exchange.

In figure A.4 we demonstrate the interplay between the τ_{AA} and τ_{BA} processes for the crystal containing 3% of admixtures. The spectrum at the lowest temperature (308 K) is determined by the motion inside the F_A sublattice. For higher temperatures the exchange motion τ_{BA} becomes progressively more important. In a certain temperature range the experimental spectra carry information about both the processes τ_{AA} and τ_{BA} ($T = 318$ and 328 K). Finally the inter-lattice exchange takes control over the lineshape ($T = 338$ and 348 K). Even though there are no dramatic differences between the particular spectra, they are very sensitive to the parameters τ_{AA} and τ_{BA} in this motional regime, and a systematic treatment leads to consistent results.

Figure A.5 shows some fluorine spectra for the crystal with the highest concentration of admixtures $x = 16\%$. Comparing the spectrum at $T = 333$ K with the spectra from figure A.4

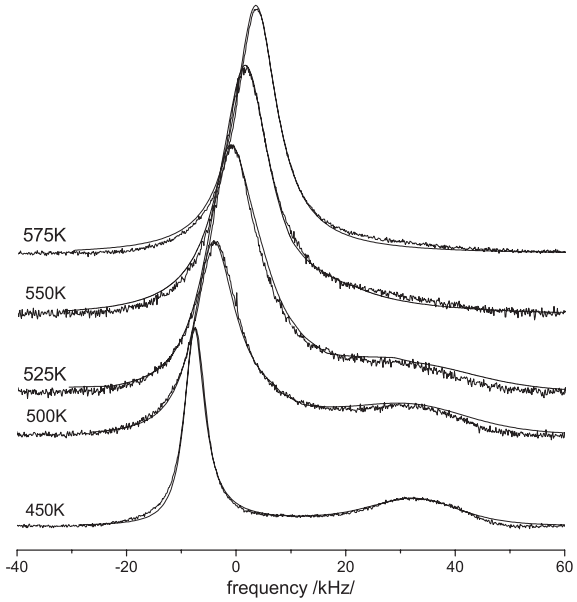

Figure A.2. Experimental and calculated fluorine spectra for a LaF_3 crystal containing 0.3% Sr^{2+} admixtures in the temperature range 450–575 K. All the spectra are modelled only by the inter-lattice exchange if one assumes that τ_{AA} is at least of the order 10^{-7} s. The exchange lifetimes τ_{BA} obtained from the least square fit are: 450 K: $\tau_{BA} = 3.6 \times 10^{-5}$ s, 500 K: $\tau_{BA} = 1.7 \times 10^{-5}$ s, 525 K: $\tau_{BA} = 6.4 \times 10^{-6}$ s, 550 K: $\tau_{BA} = 3.2 \times 10^{-6}$ s, 575 K: $\tau_{BA} = 2.55 \times 10^{-6}$ s.

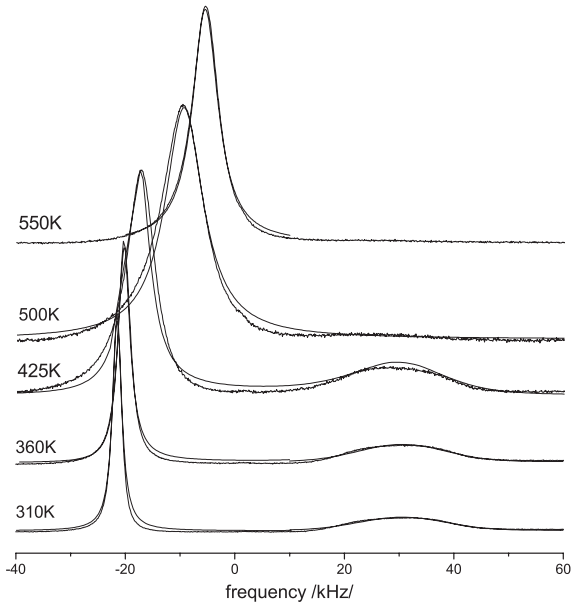

Figure A.3. Examples of fluorine spectra for a LaF_3 crystal with $x = 1\%$. The spectrum at $T = 310$ K is determined by the motion of the fluorine ions inside the F_A sublattice. For higher temperatures the spectra are modelled merely by the inter-lattice exchange encoded in the correlation time τ_{BA}. The theoretical parameters are: 310 K: $\tau_{AA} = 1.3 \times 10^{-6}$ s, $\tau_{BA} = \infty$, 360 K: $\tau_{BA} = 6.5 \times 10^{-5}$ s 425 K: $\tau_{BA} = 1.1 \times 10^{-5}$ s, 500 K: $\tau_{BA} = 3.1 \times 10^{-6}$ s, 550 K: $\tau_{BA} = 1.2 \times 10^{-6}$ s.

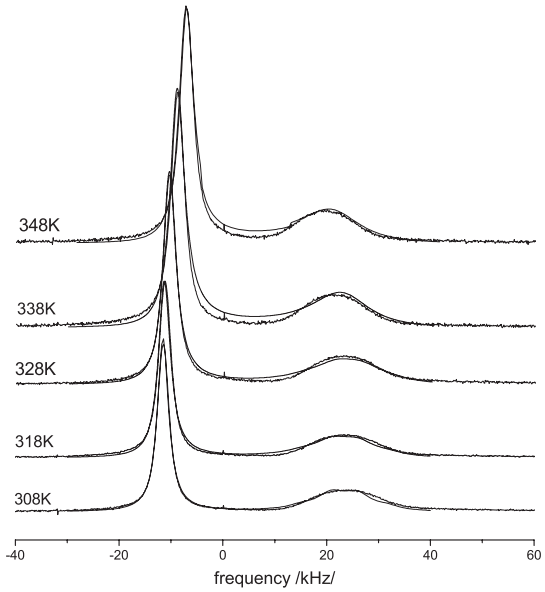

Figure A.4. Experimental and calculated fluorine spectra for a LaF_3 crystal containing 3% of admixtures. The spectrum at $T = 308$ K is determined by the fluorine motion inside the F_A sublattice. The next two spectra ($T = 318$ K and $T = 328$ K) are modelled by τ_{AA} as well as τ_{BA}. Finally the inter-lattice exchange becomes the dominant process for the NMR lineshape. 308 K: $\tau_{AA} = 1.6 \times 10^{-6}$ s, $\tau_{BA} = \infty$, 318 K: $\tau_{AA} = 1.0 \times 10^{-6}$ s, $\tau_{BA} = 1.0 \times 10^{-4}$ s, 328 K: $\tau_{AA} = 5.15 \times 10^{-7}$ s, $\tau_{BA} = 7.0 \times 10^{-5}$ s, 338 K: $\tau_{BA} = 5.1 \times 10^{-5}$ s, 348 K: $\tau_{BA} = 4.5 \times 10^{-5}$ s.

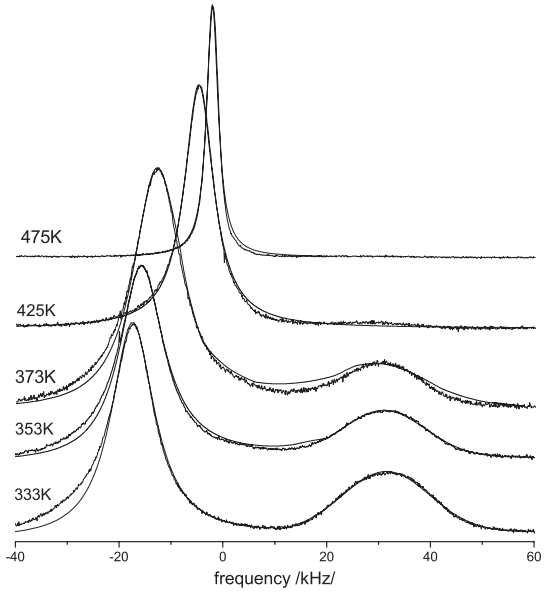

Figure A.5. Examples of experimental and calculated fluorine spectra for a LaF_3 crystal with 16% of admixtures. The parameters obtained from the least square fit are: 333 K: $\tau_{AA} = 6.85 \times 10^{-6}$ s, $\tau_{BA} = 9.55 \times 10^{-5}$ s, 353 K: $\tau_{AA} = 5.6 \times 10^{-6}$ s, $\tau_{BA} = 4.6 \times 10^{-5}$ s, 373 K: $\tau_{AA} = 3.2 \times 10^{-6}$ s, $\tau_{BA} = 2.1 \times 10^{-5}$ s, 425 K: $\tau_{BA} = 1.5 \times 10^{-6}$ s, 475 K: $\tau_{BA} = 6.05 \times 10^{-7}$ s.

corresponding to the temperature $T = 328$ or 338 K (which do not differ much from 333 K) one can conclude that the F_A line is significantly broader for $x = 16\%$. This leads to the conclusion that the motion inside the F_A sublattice is significantly slower. The timescale of this process, for $x = 16\%$, is located between the cases of $x = 0\%$ and 0.01%. Analysing the spectra one has to be aware that such a high concentration of admixtures (16%) changes the crystal structure significantly compared to the ideal one, which is used in the analysis. The structure deformation can explain the discrepancies between the experimental and theoretical F_A line (on the left side).

References

[1] Lee K and Sher A 1965 *Phys. Rev. Lett.* **14** 1027–9
[2] Sher A, Solomon R, Lee K and Muller M W 1966 *Phys. Rev.* **144** 593–604
[3] Goldmann M and Shen L 1966 *Phys. Rev.* **144** 321–31
[4] Roos A, van de Pol F C M, Keim R and Schoonman J 1984 *Solid State Ion.* **14** 191–203
[5] Geiger H, Schön G and Stork H 1985 *Solid State Ion.* **15** 155–8
[6] Maximov B and Schulz H 1985 *Acta Crystallogr.* B **41** 88–91
[7] Privalov A F, Vieth H-M and Murin I V 1989 *J. Phys. Chem. Solids* **50** 395–8
[8] Privalov A F, Vieth H-M and Murin I V 1994 *J. Phys.: Condens. Matter* **6** 8237–43
[9] Sinitsyn V V, Lips O, Privalov A F, Fujara F and Murin I V 2003 *J. Phys. Chem. Solids* **64** 1201–5
[10] Jaroszkiewicz G A and Strange J H 1985 *J. Phys. C: Solid State Phys.* **18** 2331–49
[11] Aalders A F, Arts A F M and de Wijn H V 1985 *Phys. Rev.* B **32** 5412–23
[12] Privalov A F, Lips O and Fujara F 2002 *J. Phys.: Condens. Matter* **14** 4515–25
[13] Wang F and Grey C P 1997 *Chem. Mater.* **9** 1068–70
[14] Privalov A F, Cenian A, Fujara F, Gabriel H, Murin I V and Vieth H-M 1997 *J. Phys.: Condens. Matter* **9** 9275–87
[15] Hindenach M 1997 NMR-Untersuchungen zur Ionenleitung in festen Elektrolyten *Diploma Thesis* FU Berlin
[16] Koehl P 1999 *Prog. NMR Spectrosc.* **34** 257–99
[17] Privalov A F and Lips O 2002 *Appl. Magn. Reson.* **22** 597–600
[18] Abragam A 1970 *The Principles of Nuclear Magnetism* (Oxford: Clarendon)
[19] Kimmich R 1997 *NMR Tomography, Diffusometry, Relaxometry* (Berlin: Springer)
[20] Zalkin A, Templeton D H and Hopkins T E 1966 *Inorg. Chem.* **5** 1466–8
[21] Bloembergen N, Purcell E M and Pound R V 1948 *Phys. Rev.* **73** 679–712